Preventing Thermal Osteonecrosis through 3D Printed Ceramic Grinding Tool

Bixuan Wang, Yongjie Zhao, Gongyu Liu, Chung Ket Thein, Wei Su, Shanshan Long, Huan Qi, Peng Wei, Yinfeng He, Hao Nan Li

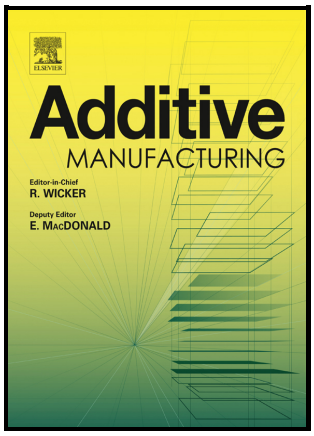

PII: S2214-8604(23)00491-8

DOI: https://doi.org/10.1016/j.addma.2023.103878

Reference: ADDMA103878

To appear in: *Additive Manufacturing*

Received date: 15 June 2023
Revised date: 13 October 2023
Accepted date: 10 November 2023

Please cite this article as: Bixuan Wang, Yongjie Zhao, Gongyu Liu, Chung Ket Thein, Wei Su, Shanshan Long, Huan Qi, Peng Wei, Yinfeng He and Hao Nan Li, Preventing Thermal Osteonecrosis through 3D Printed Ceramic Grinding Tool, *Additive Manufacturing,* (2023) doi:https://doi.org/10.1016/j.addma.2023.103878

Preventing Thermal Osteonecrosis through 3D Printed Ceramic Grinding Tool

Bixuan Wang [1,3] †, Yongjie Zhao [2] †, Gongyu Liu [1] †, Chung Ket Thein [1,3], Wei Su [4], Shanshan Long [3], Huan Qi [5], Peng Wei [4 #], Yinfeng He [1,6 #], Hao Nan Li [1,3 #]

[1] *Nottingham Ningbo China Beacons of Excellence Research and Innovation Institute, Ningbo 315100, China*

[2] *Faculty of Mechanical Engineering & Mechanics, Ningbo University, Ningbo 315211, China*

[3] *Faculty of Science and Engineering, University of Nottingham Ningbo, Ningbo 315100, China*

[4] *Institute of Biomaterials, Ningbo First Hospital, Ningbo 315010, China*

[5] *Advanced Materials Additive Manufacturing Innovation Research Center, Hangzhou City University, Hangzhou 310015, China*

[6] *Centre for Additive Manufacturing, Faculty of Engineering, University of Nottingham, Nottingham NG8 1BB, UK*

† These authors contributed equally to this work

 # Corresponding authors:

Haonan.li@nottingham.edu.cn (Prof. Li)

Yinfeng.He@nottingham.edu.cn (Prof. He)

weipeng@nbu.edu.cn (Prof. Wei)

Abstract:

Conventional grinding tools in orthopedic surgery and neurosurgery are solid in structure, leading to a limited amount of coolant that can reach the bone surgery zone, and therefore causing localized high-temperature-induced issues (infection, necrosis, and complications). Additive manufacturing allows the incomparable design and manufacturing freedoms and offers the opportunity to redesign the surgery tool to suppress the grinding temperature within a safe range. Here we present a hollow ceramic grinding tool enabled by additive manufacturing. Our CFD simulation and experiments have proved that, owing to the new design, the coolant can better reach the surgery zone, not only helping to restrict the heat accumulations, but also to remove excessive bone debris. In the *in vivo* test, we found that, the new design produced less apoptosis and edema area to the rat brain in comparison

with the conventional tool. This design minimizes the occurrence of complications such as osteonecrosis due to high surgical temperatures, opening new opportunities for the development of orthopedic surgical tools using additive manufacturing technology.

Keywords: 3D printing, grinding tool, additive manufacturing, Material Jetting, orthopedic surgery

1. INTRODUCTION

Grinding is a widely used technique in orthopedic surgery for either bone removal to provide clearer access for subsequent procedures, or bone reshaping [1]. However, traditional high-speed rotating tools would generate unacceptably excessive heat between the grinding tool-bone interface, leading to localized thermal osteonecrosis, surrounding tissue damage, and further severe consequences such as vision loss [2, 3]and nerve damage [4]. Controlling heat is therefore especially crucial, because it not only expedites the regeneration of fractured bones but also minimizes postoperative complications [5]. Therefore, researchers have been looking for an effective and cost-efficient strategy to compress surgery heat in the past decades.

Most studies focus on improving diverse cooling strategies or coolant (saline) supply systems, including using coolant with higher pressure or flow rates [6], introducing chilled [7] or mist-based saline [8], or a combination of these approaches [9]. Nevertheless, these strategies still have limitations, such as limited volume of coolant that can reach the bone-tool interface [6] and therefore reduced heat dissipation efficiency [8], and high-cost additional coolant supply systems (nozzles, pumps, valves, etc.) [8, 9]. Alternative methods, such as using femtosecond lasers [10, 11] to cut and reshape bones, remain in the early stages of development and are not yet practical for real-world applications due to technical uncertainties or complexities.

Other studies were mainly focused on improving the grinding wheel surface and grinding strategy. A new diamond wheels coated with submicron-sized titanium dioxide particles were developed to enhance the hydrophilicity of the wheel surfaces [12]. This hydrophilic grinding wheel was proven to be effective in suppressing the heat generated during grinding. However, it cannot stably inhibit the rise of temperature. To fill this gap, a grinding method that requires both cooling of the grinding point and suppression of chip adhesion on the grinding wheel surface is proposed [13]. This method can

stably inhibit the temperature rise during bone grinding without considering the rate of coolant supply.

In contrast to existing studies, we propose a redesigned hollow grinding tool that facilitates much more saline that can flow into tool-bone interface, thereby accelerating heat dissipation and controlling local temperature increase. Instead of traditional manufacturing methods like moulding, this new tool concept is fabricated via Additive Manufacturing (AM) techniques. As a well-known advanced manufacturing method in the 21st century, AM has been widely recognized for its ability to create extremely complex biomimetic porous designs unattainable through other techniques [14-17]. Li *et al.* [18] and Tian *et al.* [19] utilized 3D printing technology to design and prepare metal-bonded grinding tools with interconnected pores and liquid channels, and observed smaller grinding forces and improved grinding performance. Zhang *et al.* [20] fabricated 3D-printed polishing tools with tunable removal characteristics based on functionally-graded lattice structures. Inspired by these studies, we explore the potential of combining hollow structures with the enhanced cooling strategy in bone grinding to benefit the orthopedic surgery and neurosurgery.

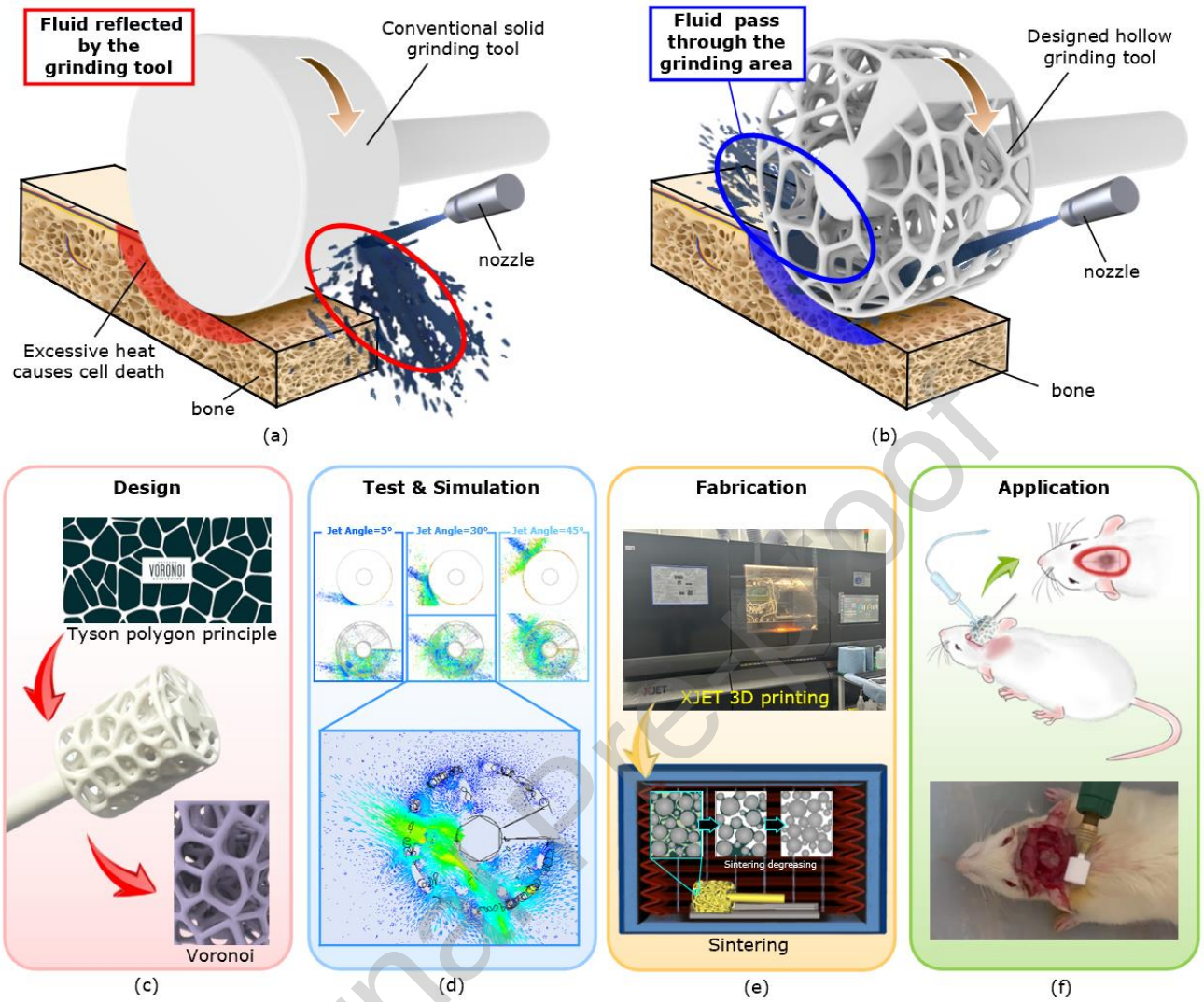

Figure 1: Conceptual diagram of (a) conventional solid grinding tool and (b) the proposed hollow grinding tool, and the methodology that we followed to design, fabricate and verify our proposed hollow grinding tool: (c) design grinding tool with 3D Voronoi principle, (d) testing & simulation for the coolant flow penetration, (e) fabrication of designed grinding tool, and (f) verification of the grinding tool performance.

Unlike conventional solid grinding tools used in surgery bouncing back a majority amount of coolant (Figure 1a), the hollow structure of our grinding tool allows the coolant to penetrate the tool and then flush the tool-bone interface (Figure 1b), reducing heat accumulation and aiding in the removal of bone debris generated during the surgery. A 3D Voronoi optimized zirconia grinding tool was designed (Figure 1c) and successfully fabricated by using Nano Particle Jetting (NPJ) approach (Figure 1e). The new design was tested both *in vitro* and *in vivo*, demonstrating promising performances (Figure 1f). This design not only helped preserve tissue viability at and around the grinding location

but also minimize the risk of infection and hyperostosis caused by debris, opening new opportunities for utilizing AM techniques in the development of orthopedic surgery tools.

2. The tool concept and structure

3D Voronoi was used to design the basic structure of the proposed grinding tool considering this structure can reach a good balance between high structure strength [21] (to serve as a surgery tool) and decent porosity (to allow coolant to penetrate). The grinding tool geometry had the head with the diameter of 10mm, the length of 12mm, and the rod with the diameter of 3mm. More specific parameters of the designed hollow grinding tool were shown in Supplementary table S1. The hollow grinding tool model was created by software Rhino and plug-in Grasshopper (version 7.20.22193), and then was exported to STL file.

Our designed grinding tool, as illustrated in Figure 2, has two grinding regions: the scaffold region (see Figure 2, blue area) and the solid region (see Figure 2, yellow area). The majority of the grinding tool consists of a reticular scaffold structure, which allows coolant fluid pass through the tool body and reach the grinding zone (see Figure 2, light blue line), effectively dissipating grinding-induced heat. Although more debris (small chips) might be generated during grinding, the effective penetration of the coolant fluid facilities the continuous flushing on these chips, ensuring that performance is not adversely affected.

To enhance grinding efficiency, we also introduced a circular solid sector. The solid region is designed to provide enhanced material removal ability during surgery, while the reticular scaffold region primarily offers auxiliary grinding, which contributes to micro-material removal and flatness improvement of the machined surface. The size of the solid region was controlled to balance bone removal efficiency and cutting fluid permeability.

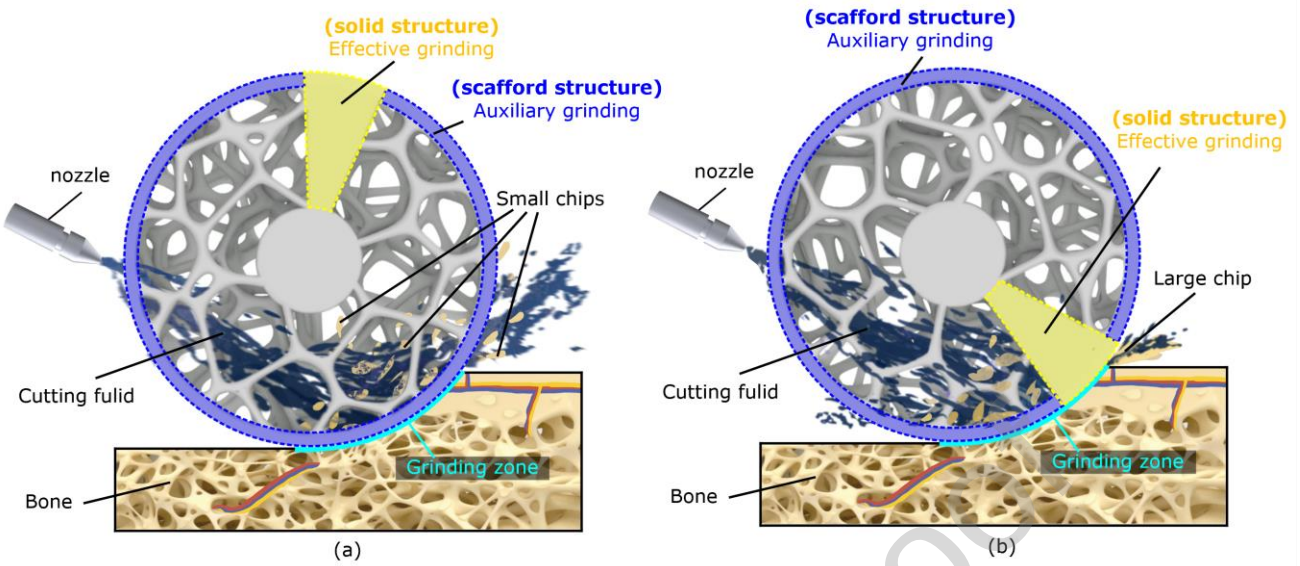

Figure 2: A schematic of the proposed hollow grinding tool having: (a) scaffold structure aiming for coolant penetration (auxiliary grinding) and (b) solid structure aiming for effective material removal (effective grinding)

3. The Coolant flow penetration

3.1 CFD simulation

To confirm that our design offers better coolant permeability, we employed CFD modeling to simulate the path of cutting fluid while the grinding tool is rotating in operation. A Computational Fluid Dynamics (CFD) analysis was performed to simulate, understand, and predict the airflow behaviors and the coolant spreading of the air-coolant two-phase system. The 3D transient interactions between the spray droplets and surrounding air were modelled by using the Euler/Lagrange approach. The most used turbulence model in engineering problems, the Discrete Phase Model (DPM), was chosen based on the application's requirements for droplet size and concentration [22, 23]. The nozzle generated droplets with the average droplet size of 50 µm [24] to capture the process details as many as possible. The timestep was set to 1e-5s to ensure the Courant number less than 1, and the rotating speed was set to 523 rad/s, corresponding to the experimental condition of 6000 rpm. All the CFD simulation was performed via ANSYS Fluent 2021R.

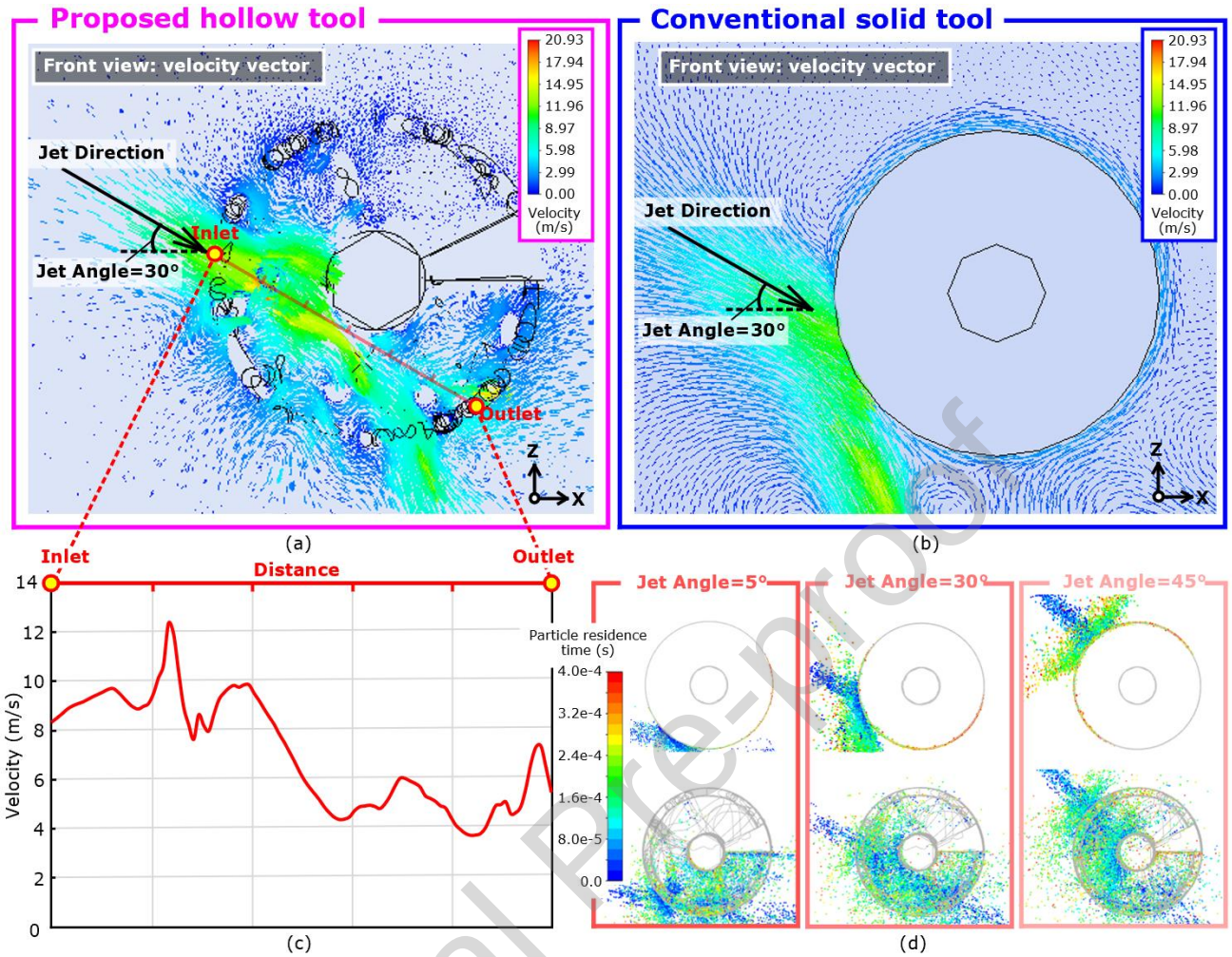

Figure 3: Simulated result of the coolant behaviours: (a) the velocity vector of the proposed hollow grinding tool and (b) conventional solid grinding tool from the front view; (c) the average fluid velocity along the path from inlet to outlet along the jet direction by using proposed tool; (d) permeability of the coolant at different jet angles (5°, 30°, 45°).

The coolant velocity vector comparison from the front view revealed interesting and unique phenomena: (i) In our design (Figure 3a), most of the cutting fluid can pass through the grinding tool body, and 48% of the employed coolant can reach the grinding zone. For the conventional solid grinding tool (Figure 3b), on the contrary, the majority of the coolant fluid bounces back. This means the proposed tool has the great potential to lower down surgery temperature; (ii) the conventional solid grinding tool has more fluid spatter than the proposed hollow grinding tool (as seen from the arrows indicating moderate velocity in Figure 3a and Figure 3b). This indicates the hollow grinding tool provides a clearer view for surgeons during surgery than the one that conventional solid grinding tool can provide; (iii) The flow rate of the coolant increased significantly after entering the hollow grinding tool, which might be caused by the impact of the coolant and the small pillar inside the

hollow grinding wheel; (iv) At the point where the fluid is ejected from the hollow grinding tool, the velocity of the coolant is reduced by only 35% compared to the velocity at the inlet (Figure 3c). This ensures better heat control ability and bone debris removal based on the proposed hollow tool.

To examine the permeability of the coolant at different jet angles, three angles (5°, 30°, 45°) were simulated (see Figure 3d). Models for the solid grinding tool using the same outer parameters were also generated for comparison. From Figure 3d, it can observe that for our tool, the coolant fluid can reach the grinding zone regardless of the used jetting angle. However, for the conventional solid tool, only the 5° jetting angle demonstrated limited fluid permeability. From the simulations, we confirmed that compared to the traditional tool, the porous mesh optimized hollow grinding tool offers better permeability for the coolant fluid and greater operational freedom for surgeons, as they can use a wide range of jetting angles. This flexibility could be crucial in some cases when surgeons need to access challenging locations or directions.

3.2 Experimental investigation

3.2.1 Setup

In order to validate whether our proposed hollow tool has a better coolant permeability than conventional solid tool, a coolant flow penetration validation experiment was performed in this study. The experimental setup is shown in Supplementary Figure S2, resembling to the standard mechanical grinding system having XYZ motion elements, spindle, tool, coolant supply and protection system. A special testing stage was designed, having a 2 mm hole on the top surface connecting to the chamber in the stage. A pH paper (San S) was placed in the chamber, right under the exit of the 2 mm hole (see Figure 4b). No clearance was existed between the tool and the hole entrance to avoid fluid enter the hole from the sides. The designed hole was small in diameter to set a strict requirement when evaluating coolant permeability for tools: Based on this test platform, the pH color will not be changed if the grinding tool has poor ability to transport coolant to reach the tool-hole interface. On the contrary, for our proposed tool, the coolant is expected to reach the grinding interface, enter the hole, then wet the pH paper, and trigger color change. Because the focus is to test the coolant behaviours in the trials while no physical contact would happen, the grinding tools were 3d printed by using transparent resin materials, which can provide a clear view of the flow behaviors and trajectories. The coolant (soda water with red paint for easy observation) was jetting towards the

rotating tool. The grinding tool was running at 6,000 rpm. The coolant (100:4:1 ratio of water to baking soda to red paint) was ejected from the nozzle at a flow rate of 10 L/min.

3.2.2 Results and discussion

Figure 4a shows the evaluation result of the coolant flow penetration. For the conventional tool, the colour of the pH paper did not change after 20 seconds, indicating no coolant reaching the grinding zone. This echoes the finds from previous CFD simulations. For the proposed tool, on the contrary, the pH test paper was immediately saturated with coolant and turned dark green when the coolant was sprayed towards the rotating tool (see Figure 4c and Figure 4d). Obviously, a large volume of coolant reaching the hole entrance with enough speed and dynamic energy. These results supported the conclusion that the hollow grinding tool had far better permeability than that of the solid tool.

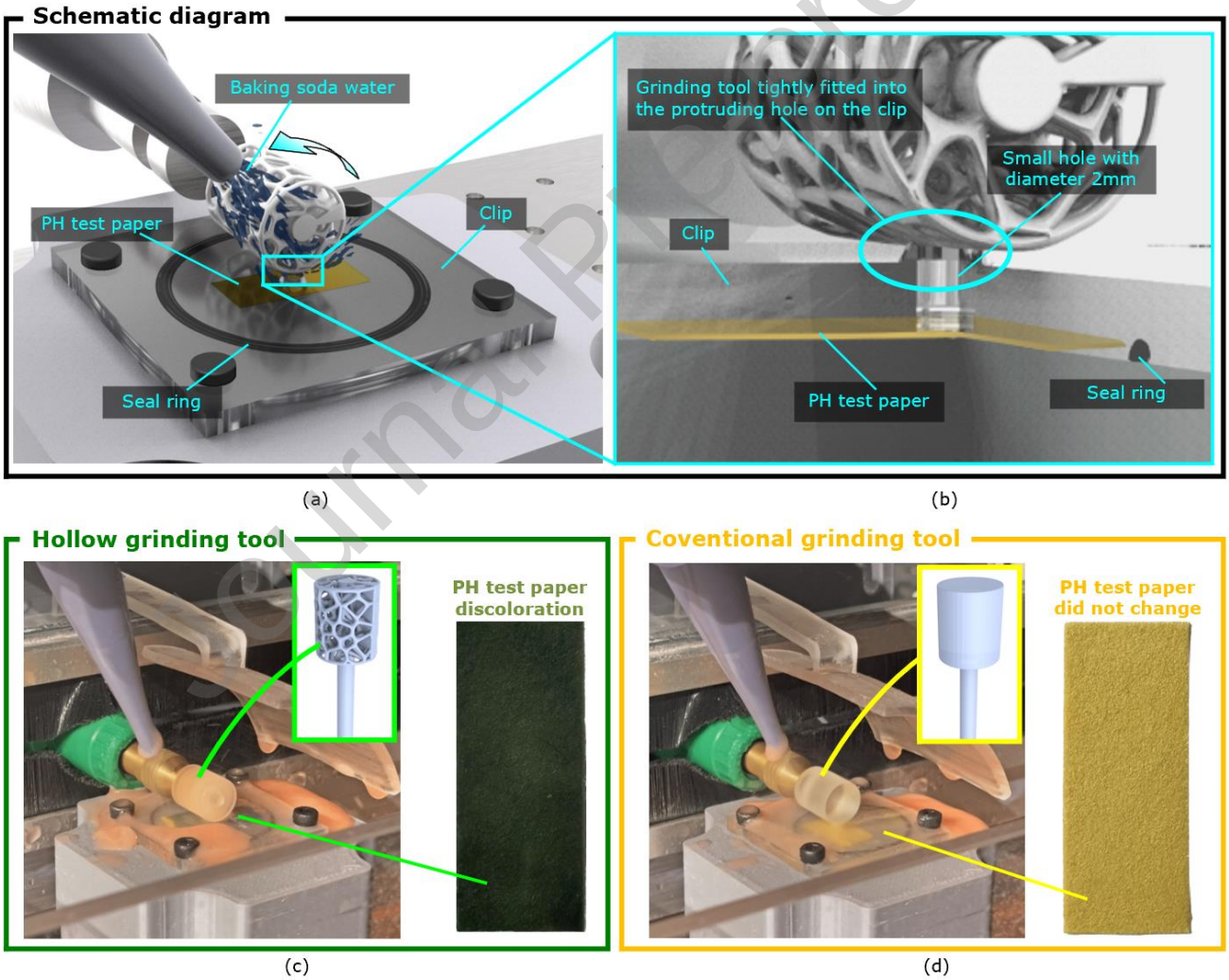

Figure 4: Permeability of the coolant fluid: (a) Schematic diagram of our setup for assessing coolant fluid flow penetration and (b) cross section view, (c) experimental process and result diagram for hollow grinding tool, and (d) conventional grinding tool.

4. The Fabrication and the geometrical/mechanical evaluation

4.1 Fabrication route

The STL model was sliced for fabrication (Supplementary in Figure S1c). A NPJ 3D Printer (XJET, Carmel 1400C, Israel, shown in Figure .1e and Figure S1c) was used for printing all the grinding tools. This system allowed the super-thin layer thickness of 10.5 µm and the jetting resolution of 1200 DPI (20 µm). Nanoparticle based structural and support inks were co-printed to form 3D structures and both inks were provided by XJET. The inks were printed onto a heated substrate (180°C) and then were scanned by using a halogen bulbs-based heating lamp to facilitate the volatilization of organic solvents in inks. A schematic of the printing process was revealed in Supplementary Figure S1. In order to compensate the shrinkage happens during the sintering, the shrinkage factor of 17.8% was applied on the designed structure [25]. After printing, the printed structure was then removed from the printing stage. The co-printed water-soluble support was removed, and the part was then sintered in a programmable sintering furnace (FMJ-19/17, FaceRom, China). After reaching the sintering temperature of 1450°C, it was held for 180 mins and then cooled to room temperature. The hollow and solid grinding tools were 3D printed by using zirconia ceramic (ZrO2), whose wear resistance is 15 times better than that of alumina ceramics, at the meantime the friction coefficient is only half of alumina ceramics.

4.2 Geometrical and mechanical evaluation

From Figure 5b and c, it can be observed that the printed tool edge surfaces showed stepped or streamlined microstructures, which enable enhanced material removal ability and grinding efficiency in surgery. Although the structures were printed with ceramic nano-particle ink, particle agglomeration was rarely observed after the sintering process suggesting completed sintering. The printed structure showed good geometrical consistency with our designs as well, although shrinkage happened during sintering.

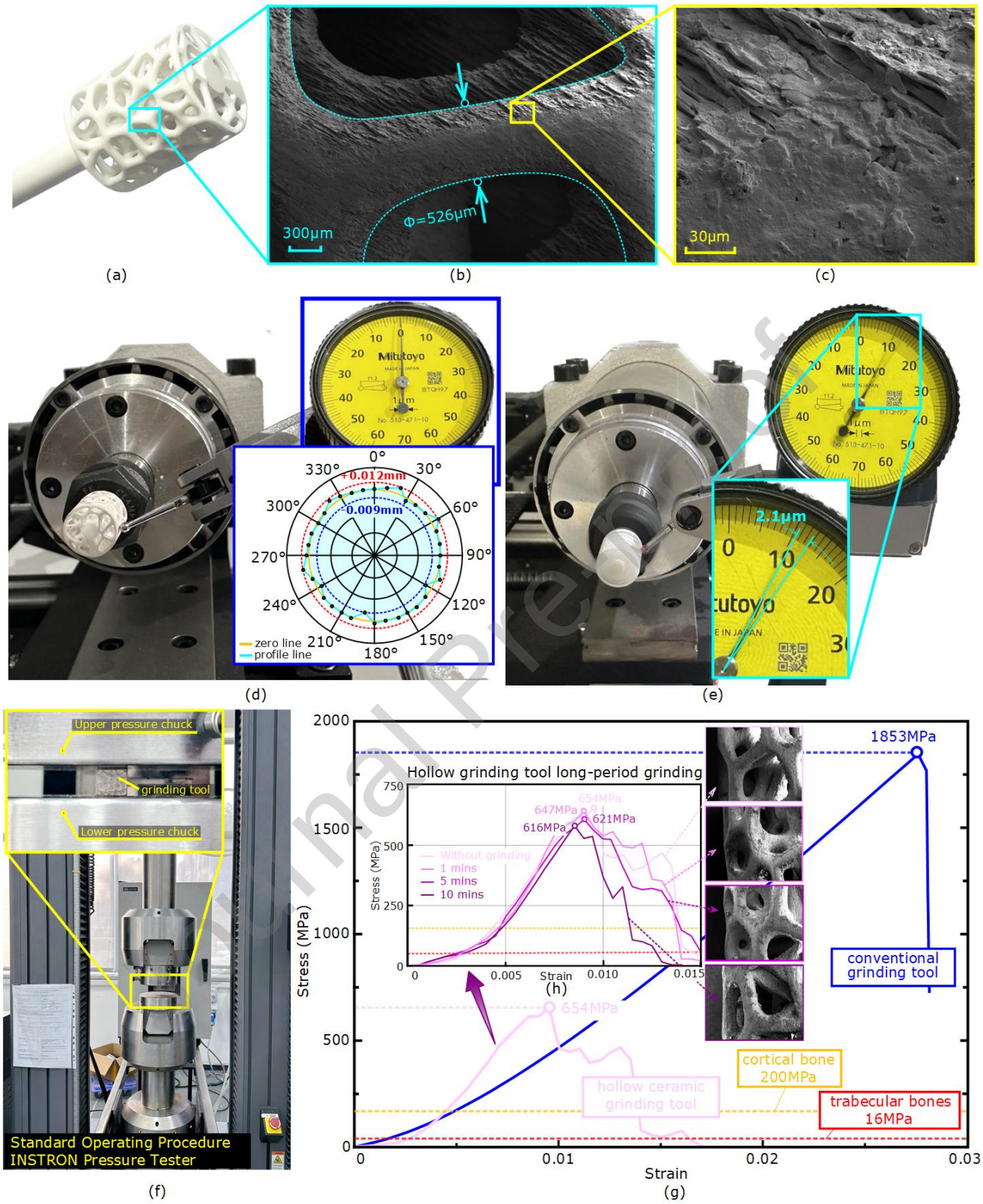

Figure 5: Evaluation of the printed hollow grinding tools: (a) sample picture and (b-c) SEM morphological images of 3D printed hollow grinding tools; (d) roundness test device and (e) dynamic balancing results; (f) tensile test and (g) obtained stress-strain curve between hollow and conventional grinding tool and (h) stress-strain curve after long-period grinding.

The circular runout was a crucial index for a rotating tool [26], and the roundness of the printed tool was tested as shown in Figure 5d. The circumferential runout ranged from +12 µm to -9 µm, only accounting for 0.21% in comparison with the tool head diameter. Except for static tool geometry accuracy, dynamic imbalance was also evaluated by observing the beating range of the dial indicator pointer, especially considering the solid portion might result in structure asymmetry. Based on our experiments, the swing range of the grinding tool during rotation is 2.1 µm. This narrow range can be negligible when considering external factors, such as hand and motor vibration in real surgery [27, 28]. As an important indicator, the mechanical performances of the printed tool were also encouraging, where the hollowed grinding tool had the ultimate strength of 654 MPa which was separately 3 times higher than that of the cortical bone (the hardest bone tissue) [29], and 31 times higher than that of the trabecular bones [30].

With the continuous grinding operation, the proposed tool strength may be reduced. To investigate the fatigue performance, we performed three runs of long-period grinding experiments with separately 1, 5 and 10 mins on bone tissue (Please note the normal period for one trial of continuous grinding operation can be no more than 1 mins [31, 32]). Based on the SEM images, the hollow tool structure did not have obvious broken and fractured failure. Based on the tensile test, the tools after a long period of grinding process have the same trend and the similar ultimate strength as that of the tool without grinding (see Figure 5h). In comparison with a new tool, the tool strength is only reduced by 5% even for the 10-minute trial, and the reduced tool strength is still larger than bone strength.

5. The in vitro assessment

5.1 Grinding temperature

A further experiment was set up to compare the temperature rise between the conventional solid and the proposed hollowed grinding tool. We designed a customized setup (shown in Supplementary Figure S3) which was similar to the setup shown in Figure S2 but with a clamping stage instead. The bone was clamped and secured by screws and plywood. The T-type thermocouple (KPS-T-0.08-2000-CZ, KAIPUSEN) was inserted into the through hole in the bone sample. The measurement junction of the thermocouples was located at the top surface of the bone sample while the other junction was connected to the data acquisition system (KPS04A0R, KAIPUSEN) (see Figure 6a). Both the solid and

hollowed tools were used to grind the bone by using the same rotation speed (6000rpm) and grinding depth (1.13mm).

It was found that the grinding temperature of the conventional solid tool stabilized at about 48.5°C, while that of the proposed hollow grinding tool at 33.3°C. The temperature for the hollow tool was 31.3% lower than that of the conventional tool, and the highest temperature was only 36.2°C. In contrast, the conventional tool achieved the highest temperature of 52.1°C, which can cause serious and irreversible damage to bone cells (According to the literature, irreversible damage can occur when the temperature at the grinding zone reaches[33, 34]).

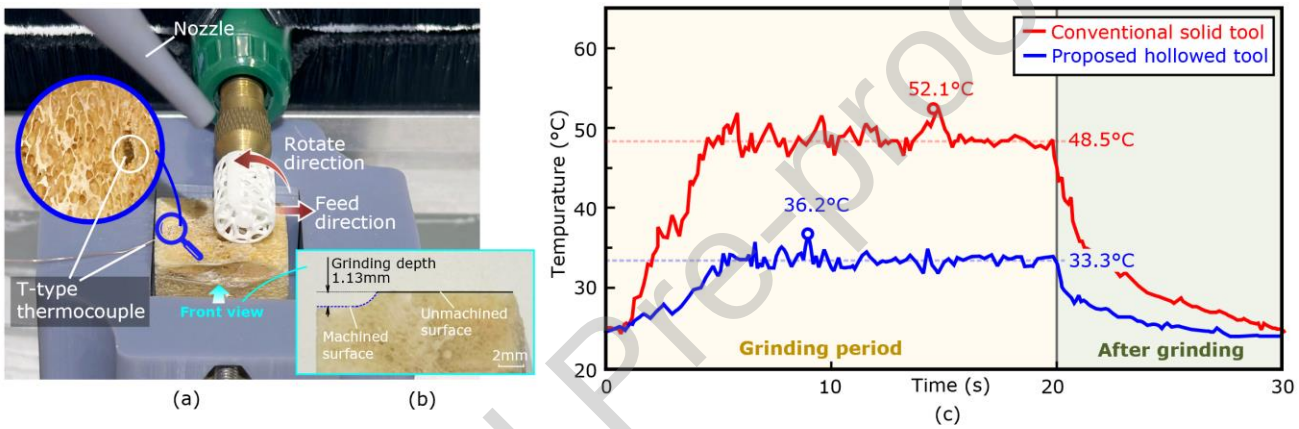

Figure 6: temperature raise assessment; (a) experiment setup, b) front view of the grinded bone and c) temperature raise result for both the solid the hollowed grinding tool.

5.2 Grinding Trial on real bone

The experimental setup of grinding trials on real bone was shown in Supplementary Figure S3. The bone was clamped and secured by screws and plywood. The grinding tool and grinder were mounted on a linear module. The grinding tool was fed along the X axis at the speed of 2 mm/min and turned counterclockwise at the speed of 6,000 rpm until the tool passed the full length of the bone. Hollow grinding tool and conventional solid grinding tool are both 3D printed ceramics.

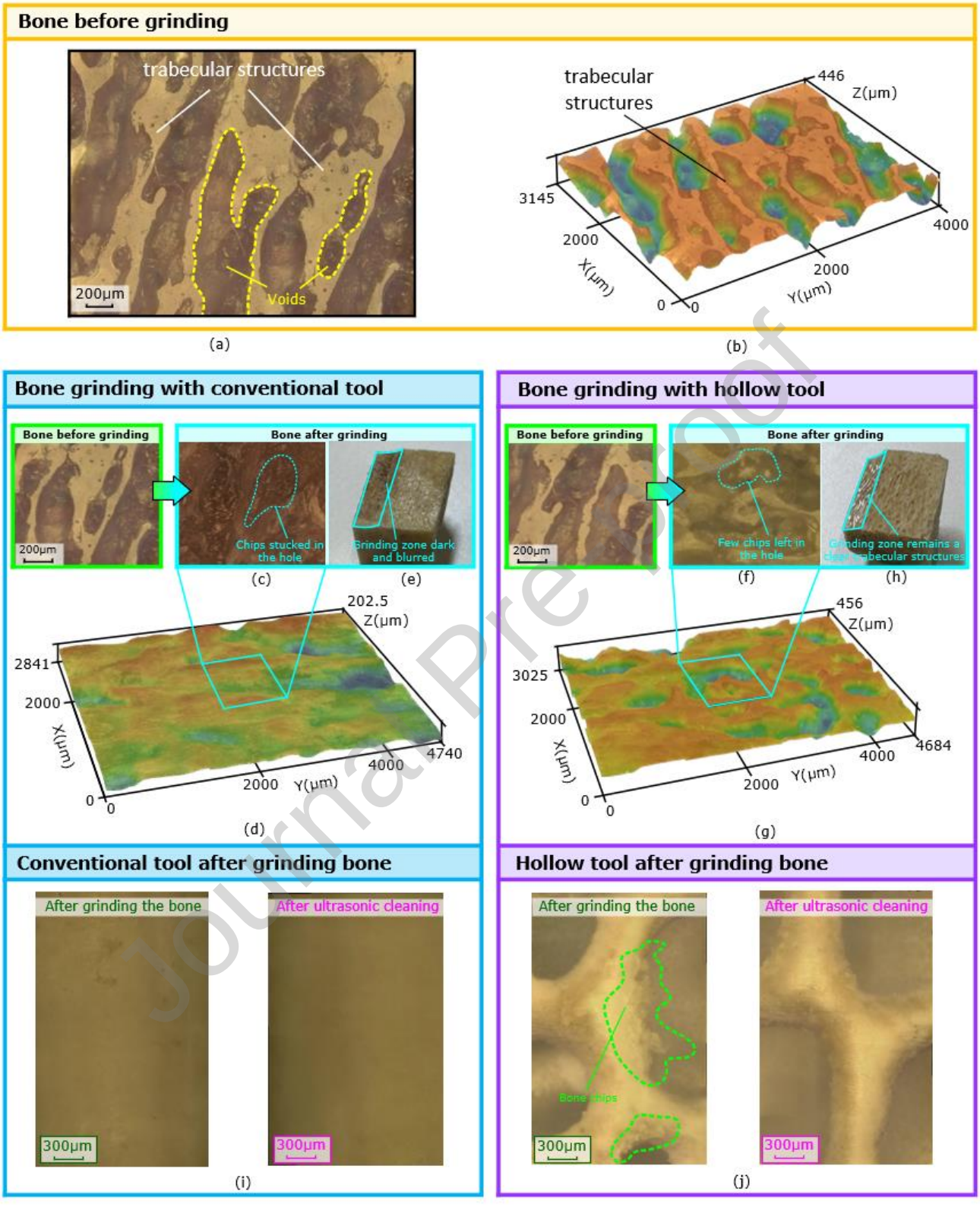

Figure 7: Comparison of the surface texture for the bone grinded with conventional solid grinding tool and hollow grinding tool: (a) 2D and (b) 3D morphology of the real bone before grinding using the 3d profilometer; (c) 2D, (d) 3D morphology and (e) real picture of the grinded bone using conventional solid grinding tool; (f) 2D, (g) 3D morphology and (h) real picture of the grinded bone

using proposed hollow grinding tool; microscopic images of (i) conventional solid grinding tool and (j) hollow grinding tool after grinding the bone.

A grinding test was also performed with a real bone from pork rib. In Figure 7a and b, it can see that the bone before grinding contained trabecular structures. When bones were grinded by conventional tools, there had a pungent odor, and the surface of the ground bones turned dark (see Figure 7e). This may be due to the high temperature during grinding denaturing the proteins, resulting in odors. The mixture containing bone protein, blood, and bone dust was generated due to this high temperature, and showed burnt smell and blurred morphologies [35]. For conventional tool, it was also observed that, most of pores between the trabecular structures in the bone were filled up with debris (see Figure 7c, d), and no bone debris were observed on the tool surface after grinding (see Figure 7j). This suggested that the debris formed during grinding were likely to be pushed into the trabecular pores and these debris may cause infections and osteosis at later stage [35]. Instead, for the bone grinded with the proposed tool, it still remained a clear trabecular structure (see Figure 7h), and only few chips were observed in pores (see Figure 7g), suggesting that the debris were brough away by both the cutting fluid and the hollow tool. A small amount of debris were found on the struts of the proposed tool after grinding (see Figure 7j), proving our statement. These debris, however, can be easily removed by a simple ultrasonic cleaning, and after cleaning the proposed tool can be used for several times with limited tool wear.

6. The in vivo assessment

6.1 Method

After confirmation of our tool ability in vitro assessment, we performed in vivo assessment to further evaluate its performances in real surgical conditions. This experiment was approved by the Ethics Committee of Ningbo University. Sprague Dawley rats aged 6 to 8 weeks were used in the experiment and divided into control group, conventional solid tool group, and proposed hollow tool group (n=6). The specific procedures were as follows: the rat was anesthetized with ketamine (60 mg/kg i.p. for rats; 100 mg/kg i.p for mice) and fixed on the animal operating table. The rat head fur was shaved off and cleaned with iodine before incision. The skin and muscle tissue of the head were cut off to fully expose the skull. The grinding tool was used to grind the rat at the same position. The temperature of the skull was recorded by infrared camera (FLIR one Pro) every second and the highest

temperature was taken until the tests were finished. After euthanizing the rats, 4 μm tissue slices were prepared according to the routine plan for the follow-up study.

After tissue sections of each group were dewaxed and rehydrated, tissue sections were stained with hematoxylin solution (Solebao Bio, China) for 10 mins, differentiated with weak acid, and then washed with distilled water. Sections were then stained with eosin solution (Solebao Bio, China) for 3 mins, then dehydrated with gradient alcohol and cleared in xylene. The optical microscope (Lecia Microsystems GmbH, Germany) was then used to observe the slices.

The apoptosis test kit (Elabscience Biotechnology, Inc., China) was used to observe the apoptosis of brain tissue cells at the grinding position. As directed by the manufacturer, tissue sections were routinely processed and incubated with TUNEL reagent (apoptotic cells showed green fluorescence), sections were counterstained with DAPI (blue fluorescence) and images were acquired using confocal microscope (Leica TCS SP5TCSSP5, Germany).

6.2 Results and discussion

For the conventional tool, before grinding the grinding region temperature was 33.3°C (Figure 8b), while after grinding the maximum temperatures reached 45.2°C (Figure 8c). For the proposed tool, as the coolant can easily reach the tool-bone interface, the temperature only reached 35.6°C (Figure 8d). This value was well below the critical temperature that can cause irreversible thermal osteonecrosis. The above statement was further confirmed by checking the brain tissue under the grinding region. Figure 8e is one example of the control group showing how a healthy brain tissue is if no grinding operation is performed. Figure 8f shows the cross-sectioned brain beneath the surgery region where grinding was performed at via conventional tool. An obvious eosinophilic change (dark blue region) was observed at the cerebral cortex accompanied by inflammatory cell infiltration. Moreover, a few edema areas were obviously visible in the deep part. As a contrast, the cross section of the brain grinded with the proposed tool did not exhibit observable changes compared to the control group. To further explore thermal damage to the neuro cells under the skull caused by different tools, Terminal deoxynucleotidyl transferase dUTP Nick End Labeling (TUNEL) staining was used to assess apoptosis of brain tissue cells. It can be found that, for the conventional tool group, the number of cerebral cortical apoptotic cells (green fluorescent) in the rat's brain significantly increased due to grinding heat induced injury (Figure 8i). However for the group with hollowed tool,

the number of apoptotic cells (Figure 8j) in the rat brain did not show noticeable increase and the status of the cells were similar to the controlled group (Figure 8h). All the above results indicated that, when grinding the skull, the use of proposed tool can effectively reduce the temperature of the skull at the grinding site and effectively avoid the damage of the underlying soft tissues.

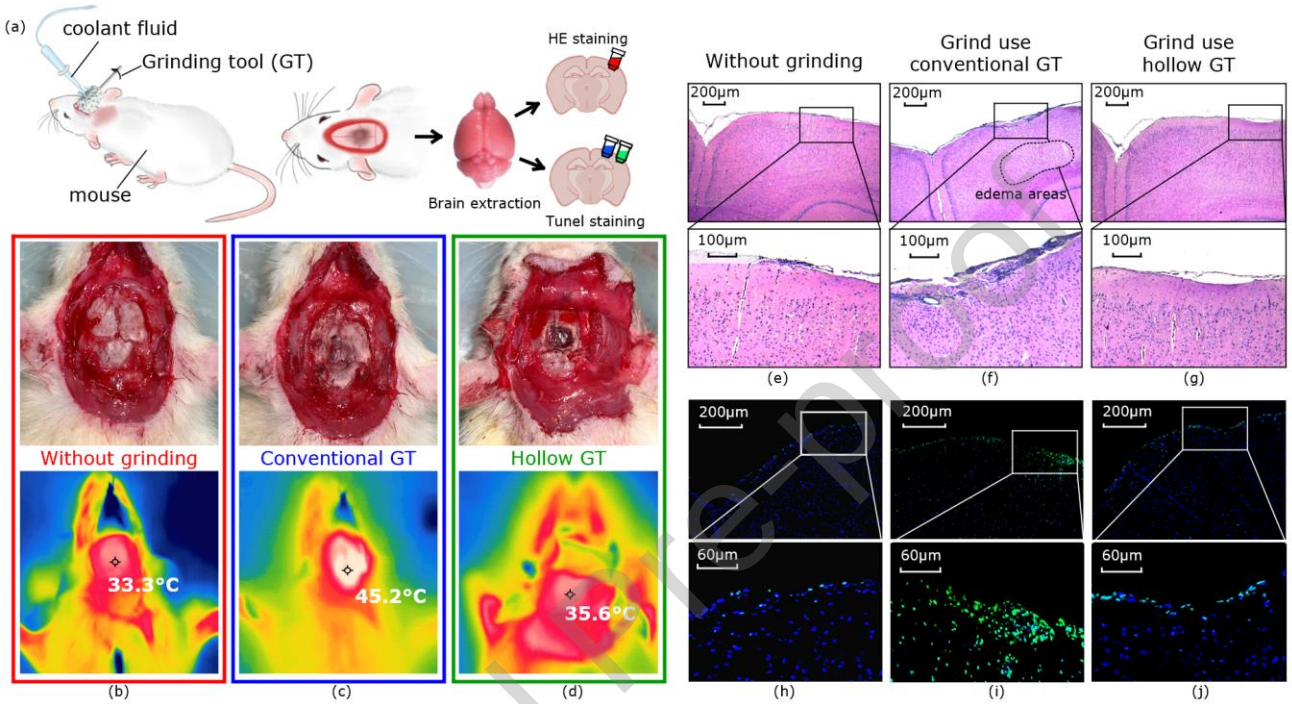

Figure 8: *In vivo* experiment designed to compare the efficiency between conventional solid grinding tool and hollow grinding tool: (a) Schematic diagram of *in vivo* assessment process; Infrared thermogram in (b) control group, (c) conventional grinding tool group, and d) hollow grinding tool group; HE staining figure in (e) control group, (f) conventional grinding tool group, and (g) hollow grinding tool group; TUNEL staining figure in (h) control group, (i) conventional grinding tool group, and (j) hollow grinding tool group.

7. Conclusion

This paper proposes a novel concept of bone grinding tool fabricated via AM. The concept can allow higher volume coolant reaching the surgery zone and lowering grinding-induced high temperature at the grinding surface. This can help minimize the symptoms such as bone necrosis caused by excessive localized temperature raise. The key findings of this work include:

(i) Based on the primary tests, for the proposed tool, 48% of coolant can reach the grinding zone, and the coolant speed was reduced by only 35% when reaching the bone-tool interface. Better flexibility

and clear vision for surgeons can be provided than the conventional tool. These statements can be proved via both CFD simulations;

(ii) Based on *in vitro* bone grinding tests, a few small bone fragments were observed in the bone trabecular structures by using the proposed tool, providing our tool effectiveness in preventing bone hyperplasia, infection caused by bone chips, and other complications in bone surgery;

(iii) Based on *in vivo* tests, grinding with our proposed tool allows the surgery temperature stabilizing at 35.6°C, which was far below the threshold temperature for bone necrosis, showing our tool ability in suppressing local heat accumulation;

(iv) Based on *in vivo* tests, less apoptotic cells and no edema areas was observed in the rat brain after skull grinding. The status of the brain was quite similar to the control group. This proved that our design is effective in preserving tissue viability during surgery.

Acknowledgements

This work was supported by Ningbo Scientific and Technological Innovation 2025 Major Project (No. 2021Z108), the National Natural Science Foundation of China (51975302, 52175417), Zhejiang Provincial Natural Science Foundation (LQ22E050014), Research Project of Key Laboratory of E&M (Zhejiang University of Technology) (EM202012014), State Key Laboratory of Mechanical System and Vibration (MSV202120), and the K. C. Wong Magna Fund in Ningbo University.

Conflict of interest

Authors declare no conflict of interest.

References

[1] L. Li, W. Han, M. Sun, B.S. Kim, X. Chen, Z.M. Aung, Z. Zhang, Y. Zhou, X. Yang, G. Chai, H. Xu, Current Practices for Esthetic Facial Bone Contouring Surgery in Asians. Clinics in Plastic Surgery, 2023. 50(1): p. 71-80.

[2] S. Singh,B. Hooda, R. Goyal, P. Taank, A case of Perioperative Visual Loss Following Spine Surgery: Can NIRS monitoring give us a clue? Medical Journal Armed Forces India, 2022.

[3] Y. Shen, M. Drum, S. Roth, The prevalence of perioperative visual loss in the United States: a 10-year study from 1996 to 2005 of spinal, orthopedic, cardiac, and general surgery. Anesthesia & Analgesia, 2009. 109(5): p. 1534-1545.

[4] V.H. De, J. Wondergem, J. Haveman, Hyperthermia-induced damage to rat sciatic nerve assessed in vivo with functional methods and with electrophysiology. Journal of neuroscience methods, 1992. 45(3): p. 165-174.

[5] N. Sugita, T. Osa, M. Mitsuishi, Analysis and estimation of cutting-temperature distribution during end milling in relation to orthopedic surgery. Medical Engineering & Physics, 2009. 31(1): p. 101-107.

[6] N. Hosono, T. Miwa, Y. Mukai, S. Takenaka, T. Makino, T. Fuji, Potential risk of thermal damage to cervical nerve roots by a high-speed drill. The Journal of bone and joint surgery. British volume, 2009. 91(11): p. 1541-1544.

[7] S. Takenaka, N. Hosono, Y. Mukai, K. Tateishi, T. Fuji, Significant reduction in the incidence of C5 palsy after cervical laminoplasty using chilled irrigation water. The bone & joint journal, 2016. 98(1): p. 117-124.

[8] M. Sasaki, S. Morris, T. Goto, K. Iwatsuki, T. Yoshimine, Spray-irrigation system attached to high-speed drills for simultaneous prevention of local heating and preservation of a clear operative field in spinal surgery. Neurologia medico-chirurgica, 2010. 50(10): p. 900-904.

[9] L. Zhang, B.L. Tai, A.C. Wang, A.J. Shih, Mist cooling in neurosurgical bone grinding. CIRP Annals, 2013. 62(1): p. 367-370.

[10] D.D. Lo, M.A. Mackanos, M.T. Chung, J.S. Hyun, D.T. Montoro, M. Grova, C. Liu, J. Wang, D. Palanker, A.J. Connolly, Femtosecond plasma mediated laser ablation has advantages over mechanical osteotomy of cranial bone. Lasers in surgery and medicine, 2012. 44(10): p. 805-814.

[11] J. Zhang, K. Guan, Z. Zhang, Y. Guan, In vitro evaluation of ultrafast laser drilling large-size holes on sheepshank bone. Optics Express, 2020. 28(17): p. 25528-25544.

[12] T. Enomoto, H. Shigeta, T. Sugihara, U. Satake, A new surgical grinding wheel for suppressing grinding heat generation in bone resection. CIRP Annals, 2014. 63(1): p. 305-308.

[13] T. Mizutani, U. Satake, T. Enomoto, A study on a cooling method for bone grinding using diamond bur for minimally invasive surgeries. Precision Engineering, 2021. 70: p. 155-163.

[14] N.S. Ha, G. Lu, X. Xiang, Energy absorption of a bio-inspired honeycomb sandwich panel. Journal of materials science, 2019. 54: p. 6286-6300.

[15] Z. Sun, S. Shi, X. Guo, X. Hu, H. Chen, On compressive properties of composite sandwich structures with grid reinforced honeycomb core. Composites Part B: Engineering, 2016. 94: p. 245-252.

[16] C. Peng, K. Fox, M. Qian, H. Nguyen, P. Tran, 3D printed sandwich beams with bioinspired cores: Mechanical performance and modelling. Thin-Walled Structures, 2021. 161: p. 107471.

[17] M. Pelanconi, A. Ortona, Nature-Inspired, Ultra-Lightweight Structures with Gyroid Cores Produced by Additive Manufacturing and Reinforced by Unidirectional Carbon Fiber Ribs. Materials, 2019. 12(24): p. 4134.

[18] X. Li, C. Wang, C. Tian, S. Fu, Y. Rong, L. Wang, Digital design and performance evaluation of porous metal-bonded grinding wheels based on minimal surface and 3D printing. Materials & Design, 2021. 203: p. 109556.

[19] C. Tian, X. Li, Z. Chen, G. Guo, L. Wang, Y. Rong, Study on formability, mechanical property and finite element modeling of 3D-printed composite for metal-bonded diamond grinding wheel application. Journal of Manufacturing Processes, 2020. 54: p. 38-47.

[20] J. Zhang, R. Hong, H. Wang, 3D-printed functionally-graded lattice structure with tunable removal characteristics for precision polishing. Additive Manufacturing, 2022. 59: p. 103152.

[21] R.V. Muratov, P.N. Ryabov, S.A. Dyachkov, Dynamic domain decomposition method based on weighted Voronoi diagrams. Computer Physics Communications, 2023. 290: p. 108790.

[22] F.L Zavalan, A. Rona, A workflow for designing contoured axisymmetric nozzles for enhancing additively manufactured cold spray deposits. Additive Manufacturing, 2023. 62: p. 103379.

[23] S. Garmeh, M. Jadidi, A. Dolatabadi, Three-Dimensional Modeling of Cold Spray for Additive Manufacturing. Journal of Thermal Spray Technology, 2020. 29(1): p. 38-50.

[24] Roberts, J., et al., Analysis and validation of a CFD-DPM method for simulating dust suppression sprays. Particulate Science And Technology, 2021(459): p. 1-12.

[25] S. Zhong, Q. Shi, , High-performance zirconia ceramic additively manufactured via NanoParticle Jetting. Ceramics International, 2022. 48(22): p. 33485-33498.

[26] P. Ma, C. Zhao, X. Lu, C. Gong, X. Niu, Rotation error measurement technology and experimentation research of high-precision hydrostatic spindle. The International Journal of Advanced Manufacturing Technology, 2014. 73: p. 1313-1320.

[27] B. Davies, K. Fan, R. Hibberd, M. Jakopec, S. Harris, Acrobot-using robots and surgeons synergistically in knee surgery. in 1997 8th International Conference on Advanced Robotics. Proceedings. ICAR'97. 1997. IEEE.

[28] J. Xu, C. Wang, P. Feng, E. Jiang, F. Feng, Meso-scale cracks initiation of Nomex honeycomb composites in orthogonal cutting with a straight blade cutter. Composites Science and Technology, 2023. 233: p. 109914.

[29] D.R. Carter, D.M. Spengler, Mechanical properties and composition of cortical bone. Clinical Orthopaedics and Related Research (1976-2007), 1978. 135: p. 192-217.

[30] S.M. Ott, Cortical or trabecular bone: what's the difference? American journal of nephrology, 2018. 47(6): p. 373-376.

[31] A. Babbar, V. Jain, D. Gupta, D. Agrawal, Finite element simulation and integration of CEM43 °C and Arrhenius Models for ultrasonic-assisted skull bone grinding: A thermal dose model. Medical Engineering & Physics, 2021. 90: p. 9-22.

[32] F.D. Burstein, C. Simms, S.R. Cohen, F. Work, M. Paschal, Iliac crest bone graft harvesting techniques: a comparison. Plastic and reconstructive surgery, 2000. 105(1): p. 34-39.

[33] G.C. Van Rhoon,T. Samaras, P.S. Yarmolenko, M.W. Dewhirst, E. Neufeld, N. Kuster, CEM43° C thermal dose thresholds: a potential guide for magnetic resonance radiofrequency exposure levels? European radiology, 2013. 23: p. 2215-2227.

[34] H. Deramond, N. Wright, S. Belkoff, Temperature elevation caused by bone cement polymerization during vertebroplasty. Bone, 1999. 25(2): p. 17S-21S.

[35] E. Alp, D. Bijl, R.P. Bleichrodt, B. Hansson, A. Voss, Surgical smoke and infection control. Journal of Hospital Infection, 2006. 62(1): p. 1-5.

CRediT authorship contribution statement

Bixuan Wang: Writing - Original draft preparation; Experiment

Yongjie Zhao: Supervision;

Gongyu Liu: Supervision;

Chung Ket Thein: Supervision;

Wei Su: Medical guidance; in vivo assessment;

Shanshan Long: Simulation;

Huan Qi: Fricabition; Resource

Peng Wei: Medical guidance; Resource

Yinfeng He: Supervision; Writing - Reviewing and Editing.

Hao Nan Li: Supervision; Writing - Reviewing and Editing.

Declaration of Competing Interest

(1) No actual or potential conflict of interest (including any financial, personal or other relationships with other people or organizations exists) in this submission;

(2) This paper is the original research that has not been published previously nor is under consideration for publication elsewhere, in whole or in part;